INSTITUTE OF PHYSICS PUBLISHING and INTERNATIONAL ATOMIC ENERGY AGENCY NUCLEAR FUSION

Nucl. Fusion **43** (2003) 989–998 PII: S0029-5515(03)67257-1

Correlation between ion/electron distribution functions and neutron production rate in spherical inertial electrostatic confinement plasmas

H. Matsuura, K. Funakoshi and Y. Nakao

Department of Applied Quantum Physics and Nuclear Engineering, Kyushu University, Hakozaki, Fukuoka 812-8581, Japan

E-mail: mat@nucl.kyushu-u.ac.jp

Received 21 January 2003, accepted for publication 22 July 2003
Published 1 September 2003
Online at stacks.iop.org/NF/43/989

Abstract

Correlation between ion/electron distribution functions and device performance, i.e. potential structure, density profile and neutron production rate, in spherical inertial electrostatic confinement plasmas is studied by solving the Poisson equation for various deuteron and electron distribution functions. For several combinations of the ion and electron convergences, dependence of the total neutron production rate on discharged current is discussed. It is shown that when electrons have high convergence and energetic component compared with ions, the neutron production rate can increase in proportion to more than a power of the discharged current, even if the neutron production is sustained mainly by the fusion reactions between the beam (deuteron) and background (deuterium) gases.

PACS numbers: 52.58.Qv

1. Introduction

The spherical inertial electrostatic confinement (SIEC) is a concept for electrostatically confining high-energy fuel ions in a spherical potential well. In the device, ions are accelerated toward the centre of the sphere, and are decelerated outward in the interelectrode space. The ions converge towards the centre of the device, and their space charge forms a virtual anode [1]. The cold electrons emitted from the cathode also converge towards the virtual anode, and are thought to create a virtual cathode inside the virtual anode [2]. The SIEC fusion system has intrinsic potential for earlier practical use of fusion energy as a compact and economical neutron/proton source, e.g. for medical diagnosis [3–5], detection of the anti-personal mines, space propulsion system [6] and subcritical fission reactors [7, 8], etc, and the studies to improve the system performance are now in progress.

So far, neutrons (protons) more than 10^8 n s^{-1} produced by D(d,n)^{3}He (^{3}He(d,p)^{4}He) fusion reactions have been observed on several devices [1–5, 9–13]. The world record of the neutron/proton production rate in SIEC devices using a spherical glow discharge as ion source has been improved continuously. In most of the experiment, increased current and voltage have facilitated the improvement in the production rate. The combination of higher values of the discharged current and voltage, however, causes the problem of overheating the spherical cathode. To reduce the heat of the spherical cathode, substitution of the grid wires with a spherical laminar structure whose electrostatic properties alone increase the neutron gain and reduce the heating has been proposed [14]. To further improve the device performance, however, it is important to investigate the method by not relying only on the enormous increase in the external current and voltage.

In parallel with the neutron/proton production, in some devices, the double peak in the radial profile of the neutron/proton production rate [9, 10, 13] has been measured. The appearance of the double neutron/proton peak suggests a formation of the multiple potential well inside the area within the cathode [1, 2, 9–13]. Several measurements have been made to examine the formation of a multiple potential well [1, 15]. Thorson *et al* [1] carried out an experiment to examine the existence of the virtual cathode at the centre of the sphere by directly measuring the potential using emissive probes. In their experiment, the virtual anode was observed at the centre of the sphere, whereas no virtual cathode could be seen. In recent experiments by Yoshikawa *et al* [15],

in which they estimated the potential by means of the laser-induced fluorescence (LIF) method, the appearance of the double potential well was recognized along with the existence of energetic electrons in the localized region near the potential peak. In theoretical simulations, it is predicted that the potential structure is strongly influenced by the device parameters [16], i.e. grid current and grid voltage as well as the ion and electron convergences [16–19]. In our previous calculations [16, 17], it was also shown that when electrons have a slightly higher convergence than ions, the double radial peak in the neutron/proton production rate can appear without the creation of the deep double potential well. To ascertain the characteristics of the multiple well and its effect on the device performance, it is necessary to clarify in what conditions the multiple potential appears and how the potential structure, i.e. the height and the position of the potential peak, depends on the device parameters.

On the other hand, in recent experiment using a spherical glow discharge as the ion source, an operation mode in which the neutron production rate increases in proportion to the 1.3–2.0th power of the discharged current was observed [12]. The increase in the neutron/proton production rate proportional to more than a power of the discharged current is advantageous to the device scaling. In subsequent theoretical PIC simulation [18, 19], Ohnishi *et al* pointed out that the potential well is unstable and oscillates with a period much longer than the inverse ion plasma frequency. They estimated the fusion reaction between counterflowing ions, and revealed that the intermittent peaking of the density in the central region causes higher neutron production proportional to more than the second power of the discharged current. In previous experiments, however, the fusion reaction between the beam ion and the background deuterium is considered to govern the total neutron production. To understand the previous experiment, the correlation between the neutron production rate and the discharged current should be discussed after including the effect of the beam–background fusion reactions.

The SIEC fusion device is essentially a beam-fusion system. In such a system, the velocity distribution function of the beam ion has an important bearing on system performance. In order to consistently understand the experimentally observed phenomena occurring in the SIEC plasmas and improve the device performance more rapidly, it would be necessary to understand the correlation between ion/electron distribution functions and plasma performance, as well as what distribution can appear in equilibrium SIEC plasmas and how we can control the distribution functions. In this paper, we examine the correlation between the ion/electron distribution functions and plasma performance by looking at an instantaneous plasma state for various combinations of non-equilibrium ion/electron distribution functions in SIEC plasmas where the potential structure is formed and collapsed [18, 19]. For this purpose, we introduce a model equation to express the shape of the ion and electron distribution functions. By solving the Poisson equation for presumed distribution functions, the potential structure and the density and radial profiles of the neutron/proton production rate are evaluated together with the total neutron production rate itself. Throughout the calculation a fusion reaction between the beam deuteron and the background deuterium gas is assumed. The possible mechanisms of the appearance of the operation mode in which the neutron production rate increases proportional to more than a power of the discharged current, even if the neutron production is sustained mainly by the fusion reactions between the beam deuteron and the background deuterium gas, is discussed along with the condition to attain such an operation mode.

2. Analytical model

The SIEC fusion device is a weak collisional system, where the collision frequency and fusion reaction rate are small compared with the transit frequency of charged particles in a given electrostatic potential. The motion of a charged particle in such a system is described by two constants of motion: the total energy $E = \frac{1}{2}mv^2 + q\phi$ and the angular momentum $L = mrv_\perp$. In these systems, the distribution functions of charged particle can be expressed as an arbitrary function of E and L [17–21]. In this paper, we describe the SIEC device in the spherical coordinates and assume the spherical symmetry of the device. The ion and electron distribution functions are assumed to be functions of only E and L, i.e. $f(E, L)$; we assume the function does not explicitly depend on the radial position r in the spherical device. In previous works, using this assumption, attempts were made to express the shapes of the distribution functions by using, for example, the δ and/or the Heaviside functions [18, 20]. In this case, however, the radial profiles of potential and density tend to have an unnatural shape, including the mathematically discontinuous point. This would be attributed to the peculiarity of the δ and/or the Heaviside functions. To resolve this problem, we simulate the distributions using the exponential function so that their shapes are close to those expressed by the Heaviside function. The weak Coulomb collision may slowly relax the distributions towards a Maxwellian process. The timescale in which the distribution broadens would be larger in the energy space than in the angular momentum space. The electrons are assumed to be generated with low kinetic energy at the cathode. As a model equation, we, therefore, introduce the following form of the ion and electron distribution functions [17] by using dimensionless parameter α_a, β_a and ξ_a, to examine how the system characteristics are influenced by the distribution function,

$$f_a(E, L) = c_a \exp\left[-\left(\frac{E - \xi_a|q_a\phi_0|}{\alpha' q_a\phi_0}\right)^2 - \left(\frac{L}{\beta_a L_0^a}\right)^2\right], \tag{1}$$

where subscript a represents particle species, i.e. deuteron or electron, ϕ_0 the grid voltage and $L_0^a = r_{\rm cat}\sqrt{2m_a\phi_0}$. By adjusting the α', β_a and ξ_a values, we can simulate the broadness of the distributions in the energy and angular momentum spaces. Throughout the calculations, $\alpha' = \alpha(E < |q_a\phi_0|)$ and $0.1(E \geqslant |q_a\phi_0|)$ are assumed. The α' and β simulates the broadness of the ion/electron distribution towards energy and angular momentum directions. When $\alpha'(\beta) \to 0$, the distribution function is close to the δ-function. Small β values represent the high-converged ion/electron distribution functions. On the contrary, when $\alpha'(\beta) \to \infty$ the ion/electron has uniform distribution in

the energy (angular momentum) space. ξ_a represents the position of the energy peak of the distribution functions. When $\xi_a = 1$, the ion/electron has a peak at the same energy as the externally discharged potential energy. The coefficient c_a is determined so that the deuteron (electron) density at the cathode $n_i(r_{cat})$ ($n_e(r_{cat})$) is equal to $n_i^{cat}(n_e^{cat})$. In this note, following Thorson's treatment [1, 22], we relate n_i^{cat} to the measured cathode current I_{meas} by

$$n_i^{cat} = \frac{1}{1-\gamma^2}\frac{1}{1+\delta}\frac{I_{meas}}{4\pi r_{cat}^2\sqrt{2e\phi_0/m_D}e}, \tag{2}$$

where γ represents the transparency factor of the inner grid [2] and δ is the number of secondary electrons emitted from the grid due to ion impact [1]. Throughout the calculation $\delta = 1$ [1] is assumed. We consider the secondary electrons emitted from the cathode with low kinetic energy, $\phi_e = 5\,\mathrm{eV}$. These electrons would pass through the core region only once, thus n_e^{cat} is related to the measured cathode current I_{meas} by

$$n_e^{cat} = \frac{\kappa\delta}{1+\delta}\frac{I_{meas}}{4\pi r_{cat}^2\sqrt{2e\phi_e/m_e}e}, \tag{3}$$

where roughly half of all the secondary electrons are assumed to be drawn inside the cathode, i.e. the fraction of secondary electrons drawn inside the cathode κ is taken as $\kappa = 0.5$.

The electrostatic potential structure can be determined by the Poisson equation:

$$\nabla^2\phi(r) = -\frac{q_i n_i(r) - q_e n_e(r)}{\varepsilon_0}. \tag{4}$$

By integrating equation (1) using the initial potential structure, we obtain the radial profile of deuteron and electron densities. By substituting the density profiles into equation (4), we solve the Poisson equation and get the potential structure again. This process is repeated until a correct solution, i.e. potential structure, is obtained. From $f_D(E, L)$ and $\phi(r)$, the space-dependent deuteron velocity distribution function $F_D(r, v_\parallel, v_\perp)$ can be estimated. Here, $v_\parallel$ represents a radial velocity component, and $v_\perp$ is the vertical component in spherical co-ordinates. Using the velocity distribution function, the D(d,n)^{3}He fusion reaction rate coefficient is evaluated:

$$\begin{aligned}\langle\sigma v\rangle_{\mathrm{D(d,n)^3He}} = {} & \frac{\sqrt{2\pi}}{n_D}\left(\frac{m_N}{T}\right)^{3/2}\int \mathrm{d}v_N v_N \exp\left(-\frac{m_N}{2T}v_N^2\right)\\ & \times\int \mathrm{d}v_\parallel\int \mathrm{d}v_\perp \frac{v_\perp}{\sqrt{v_\parallel^2+v_\perp^2}}F_D(r, v_\parallel, v_\perp)\\ & \times\left[\int_{|v_N-\sqrt{v_\parallel^2+v_\perp^2}|}^{v_N+\sqrt{v_\parallel^2+v_\perp^2}} \mathrm{d}v_r v_r^2\sigma(v_r)\right],\end{aligned} \tag{5}$$

where $v_r = |\vec{v}_N - \vec{v}_D|$ and subscript N represents background neutral deuterium. The D(d,n)^{3}He fusion cross-sections $\sigma(v_r)$ are taken from the work of Duane [23] who assumed fusion reactions between bare nuclei. Throughout the calculations the background deuterium gas is assumed to be Maxwellian at 0.1 eV temperature. From the reaction rate coefficient and deuteron and background deuterium densities, the radial profile of the neutron production rate owing to beam (deuteron)–target (background deuterium gas) fusion is estimated.

3. Numerical results and discussions

3.1. Correlation between ion/electron distribution functions and potential structure

In figure 1, we first show the radial profiles of (*a*) deuteron density, (*b*) electron density and (*c*) electrostatic potential for several ion and electron convergences, i.e. β_D and β_e values. In this calculation ions are assumed to have the same convergence as electrons, i.e. $\beta_D = \beta_e$, and the grid voltage $\phi_0 = 10\,\mathrm{kV}$, cathode current $I_{meas} = 100\,\mathrm{mA}$ and $\alpha = 0.1$, $\xi_D = \xi_e = 1$ are chosen. Small $\beta_D(=\beta_e)$ values imply higher convergence of deuterons towards the centre of the sphere (see equation (1)). In figures 1(*a*) and (*b*), it is found that both deuteron and electron densities around the central region increase together with the potential (figure 1(*c*)) for small β values. When $\beta_D = \beta_e = 0.1$, we can observe a central sink in the deuteron density profile (figure 1(*a*)). This is because the number of deuterons that can reach the central core region decreases owing to the increased potential. Although the potential becomes large for small β values, the virtual cathode cannot be seen.

In order to grasp the correlation between ion/electron distribution functions and potential structure, calculations are

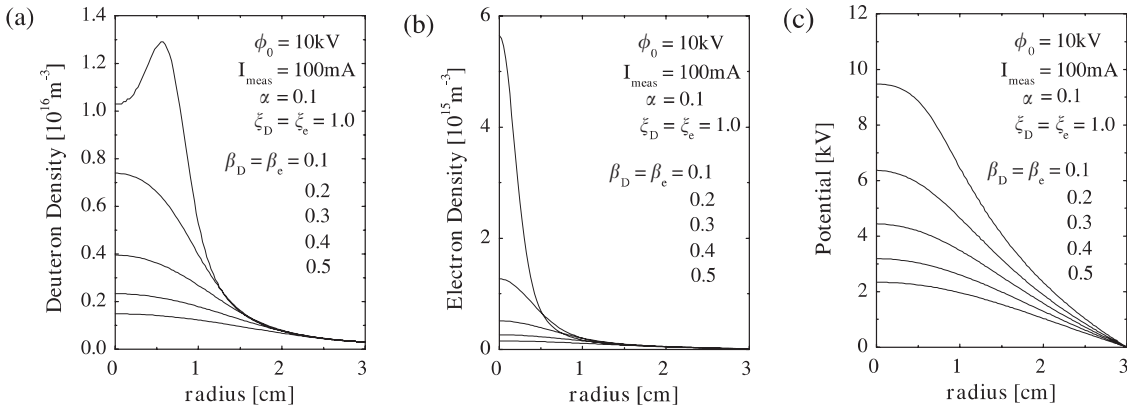

Figure 1. Radial profiles of (*a*) deuteron density, (*b*) electron density and (*c*) potential for various $\beta(\equiv \beta_D = \beta_e)$ values. In this calculation $\alpha = 0.1$ is assumed.

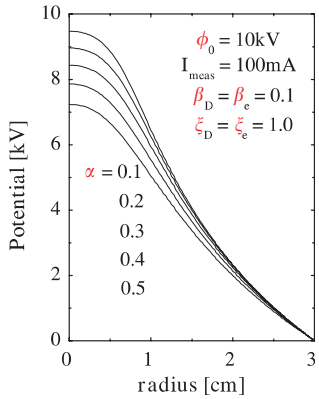

Figure 2. Correlation between distribution broadness in the energy space and potential structure.

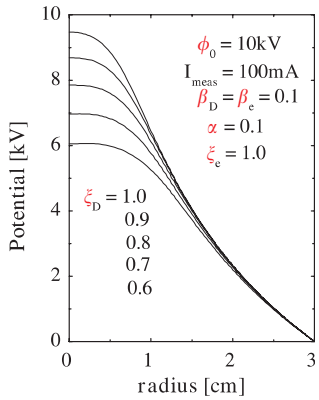

Figure 3. Effect of slowing-down of deuterons on potential structure.

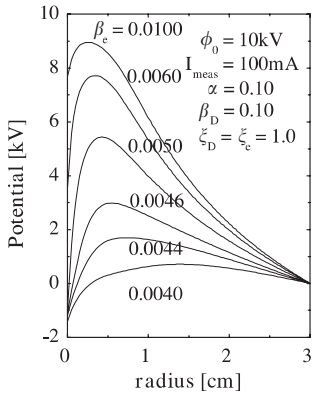

Figure 4. Potential structure for various β_e values. The virtual cathode is formed by the converged electrons (for small β_e values).

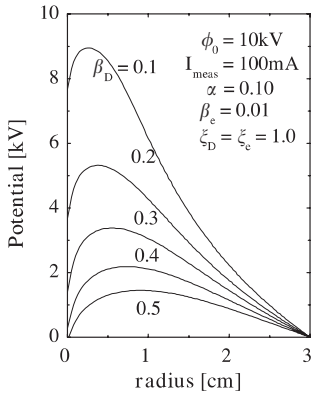

Figure 5. Potential structure for various β_D values. The virtual potential well is extended for large β_D values.

made for several adjusting parameters of distribution functions, i.e. α, ξ_a and β_a in equation (1). In figure 2, potential structures are shown for several α values. Here, $\beta_D = \beta_e = 0.1$ and $\xi_D = \xi_e = 1$ are assumed. As ion distribution function broadens in the energy space (for large α values), the potential decreases over the complete radial range. This is because the number of deuterons that can converge in the central core region overcoming the central potential hill becomes small. By adjusting the energy peak of the deuteron distribution function, i.e. parameter ξ_D, we can simulate the influence of the energy dissipation of deuterons on the potential structure. The potential structures for several ξ_D parameters are shown in figure 3. Here, $\alpha = 0.1$, $\beta_D = \beta_e = 0.1$ and $\xi_e = 1$ are assumed. For the same reason as when the distribution broadens (figure 2), the potential decreases over the complete radial range as a consequence of the energy dissipation of deuterons.

Next, we examine the case when electrons have higher convergence than ions. In figure 4, potential structures for several β_e values are exhibited. Here, $\alpha = 0.1$, $\beta_D = 0.1$ and $\xi_D = \xi_e = 1$ are assumed. The virtual cathode can be observed at the centre of the sphere. For small β_e values, owing to the existence of the high-energy component in the electron distribution function, the potential decreases slightly below zero at the centre of the sphere. In figure 5, potential structures are indicated for several β_D values. Here, $\alpha = 0.1$, $\beta_e = 0.01$ and $\xi_D = \xi_e = 1$ are assumed. As ion convergence becomes weak (i.e. large β_D values), the position of the potential peak, i.e. virtual anode, is moved outward. This is attributed to the relative reduction of the deuteron density compared with electrons around the central region. Owing to the weak convergence of ions, the area where the virtual potential well is formed is extended. It should be kept in mind, however, that the ion density around the central core region decreases due to lower convergence of ions. The neutron production rate is determined as a result of the competition between increment (decrement) in the number of deuterons accelerated in the virtual potential well and decrement (increment) in the potential, i.e. increment (decrement) in the fusion reaction rate coefficient, for small (large) β_D values.

We now look at the plasma when ions have higher convergence than electrons. The potential structure and deuteron density profile are shown in figures 6(*a*) and (*b*), respectively. For high convergence of deuterons (small β_D values), potential raises over the complete radial range. For small β_D values, owing to the existence of the high-energy tail component in the deuteron distribution function, the potential goes over the 10 kV around the central region. Due to the increased potential, the deuteron density decreases around the central region, whereas it tends to have somewhat higher values at the centre of the sphere. This could be attributed to the geometric effect around the central region where the potential is almost flat. Here, it should be noted that as a result of the increased potential, the fusion reaction rate coefficient is considerably small around the central region, and most of the neutrons are produced near the cathode region.

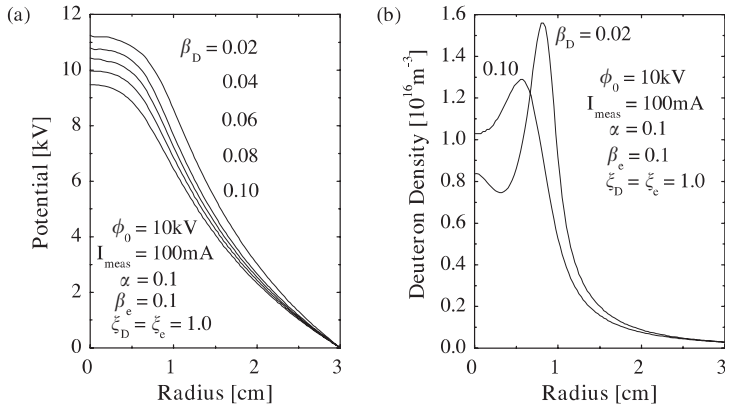

Figure 6. (*a*) Potential structure and (*b*) radial deuteron–density profile when deuterons have higher convergence than electrons.

3.2. Correlation between discharged current and neutron production rate

From the potential profile obtained and equation (1), we can estimate the velocity distribution function of deuteron at each radial point. From the space-dependent velocity distribution function [17], the D(d,n)^{3}He fusion reaction rate coefficient is evaluated, and by multiplying the reaction rate coefficient by deuteron and background deuterium densities, the neutron production rate is calculated at each radial point. The radial profile of the neutron production rate is integrated over the full area within the cathode, and the total neutron production rate is obtained. In the following sections, we examine the effect of the potential structure on the neutron production rate and the dependence of the neutron production rate on the discharged current for several combinations of ion and electron convergences.

3.2.1. Comparison of the present model with experiment. We first carry out the calculation assuming that electrons have almost the same (or lower) convergence as (than) ions. In present model, we have examined an instantaneous plasma state for various non-equilibrium ion/electron distribution functions. We have assumed that the distribution function, i.e. $f(E, L)$, does not explicitly depend on the radial position. In order that this treatment is justified, the mean free path of the charged particle must be longer than the grid radius. This condition would be barely satisfied in the deuterium gas whose pressure is less than $\sim$1 Pa (although the effect of collisional processes on total neutron production itself would begin to be appreciable in a further low-pressure range). Nevertheless, the comparison of our model with the current experiment would be useful to understand the dependence of the neutron production rate on discharged current/voltage and influence of presumed device parameters, i.e. γ, δ, on the neutron production rate.

In figures 7(*a*) and (*b*), the total (integrated) neutron production rate by D(d,n)^{3}He fusion reactions from the area within the cathode is shown for several γ values, as a function of discharged current and voltage, respectively. Here, $\alpha = 0.1$, $\beta_D = \beta_e = 0.1$ and $\xi_D = \xi_e = 1$ are assumed. The solid lines and curves show the present calculation, while the white circles denote the experimental data [10, 11]. The large grid-transparency factor (γ) implies a large circulating current, which increases the actual ion density circulating in the spherical device. This causes an increase in the neutron production rate. When ion convergence is considerably higher than electrons, the potential increases in the central core region, and owing to the deceleration of ion speed, the neutron production from the central core region becomes small. The neutron production rate is hence directly governed by the cathode density, which is determined by equation (2); thus, the total neutron production rate increases linearly with increasing current. If we choose $\gamma = 0.8$ as shown in figure 7, the present calculations approximately agree with the experiment. In figures 8(*a*) and (*b*), we next show the total (integrated) neutron production rate by D(d,n)^{3}He fusion reactions for several δ values, as a function of discharged current and voltage, respectively. Here, $\alpha = 0.1$, $\beta_D = \beta_e = 0.1$ and $\xi_D = \xi_e = 1$ are assumed. The large δ value causes an increase in the number of electrons, i.e. current carried by the electrons. In present model, to keep the total amount of current constant, ion density decreases, thus the neutron production rate also decreases with increasing δ values. As shown in equation (2), the ion density at the cathode depends explicitly neither on ϕ_e nor κ values. Although the potential structure and radial profile of the neutron production rate are influenced by ϕ_e and κ values through electron density, the influence on the total neutron production rate is small. In figure 7, the number of secondary electrons emitted from the grid due to ion impact, δ, is taken as unity. In this case, to reproduce the neutron production of the same order as experiment, we must use a low transparency factor, i.e. $\gamma = 0.8$, in the calculations. On the other hand, in figure 8 ($\gamma = 0.95$), to reproduce the neutron of the same order as in the experiment, a high electron density must be assumed. These results suggest that the current treatment has somewhat overestimated the neutron production rate. In laboratory devices, owing to the productions of the second generation low-energy ions by charge-exchange collisions [24], averaged ion-energy may be lower than that of the present model. If we aim at a more accurate comparison of the absolute values of the neutron production rate itself, more detailed information on the device, i.e. collisional processes, fusion reaction outside the spherical cathode, reaction between accelerated and grid-embedded ions, etc, should also be incorporated.

If ion distribution has considerably higher convergence in both energy and angular momentum spaces, the converged

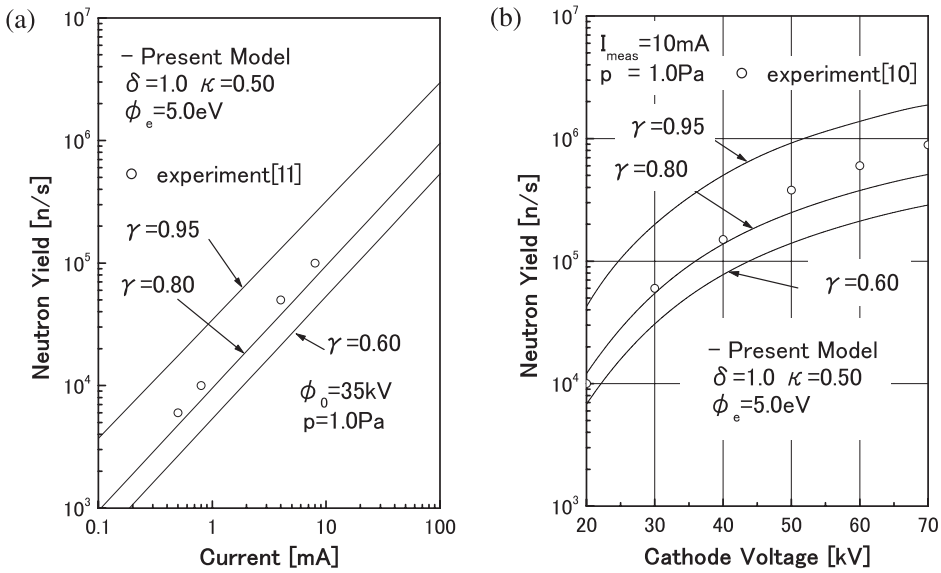

Figure 7. The dependence of the neutron production rate on discharged (*a*) current and (*b*) voltage for several γ values. The present model is compared with experiments [10, 11].

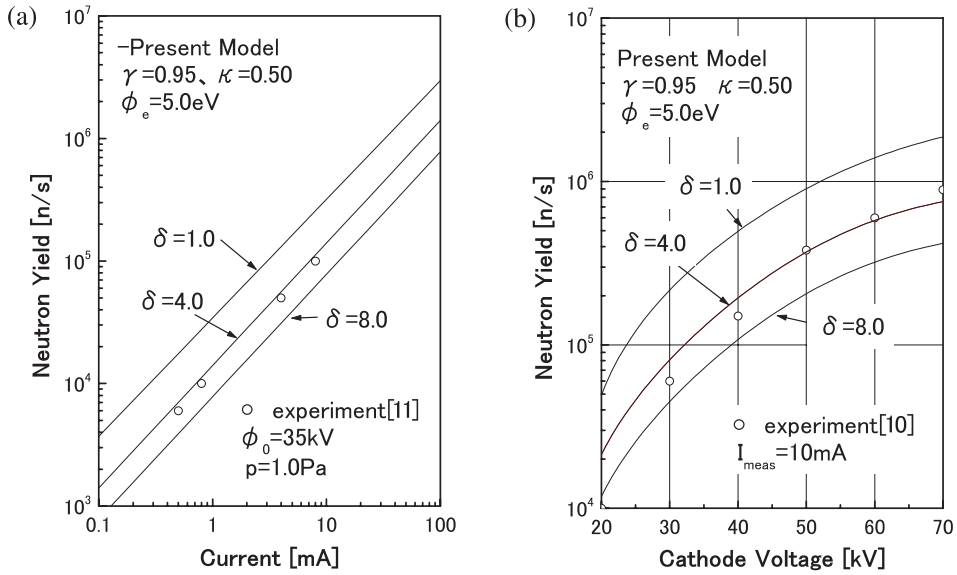

Figure 8. The dependence of the neutron production rate on discharged (*a*) current and (*b*) voltage for several δ values. The present model is compared with experiments [10, 11].

ions would create a highly increased potential hill, i.e. virtual anode, at the centre of the sphere. In this state, as presented in figure 1(*a*), the central sink in the radial density profile begins to appear. The increased potential also decelerates the ion speed, and prevents the neutron production rate from linearly increasing in proportion to a power of the discharged current. In figure 9, the neutron production rate is presented as a function of the discharged current for small $\beta_{\rm D}(=\beta_{\rm e})$ values. Both the increased current and higher convergence of ion and electron cause the rapid increase in the potential. As the potential increases, the degree of the increment in the neutron production rate gradually declines. Of course, such a result has not been reported in previous experiments. In order to reproduce the highly increased potential hill, perfectly collision-less plasma, small electron concentration and completely spherical symmetry of the device would be necessary, in addition to considerably higher convergence of ions. In subsequent sections we continue the discussion excepting for such an ideal device condition, i.e. considerably increased potential.

3.2.2. Radial profile of neutron production rate. When electron convergence is higher to some extent than that of ions, e.g. $\beta_{\rm D} \approx 10\beta_{\rm e}$, most of the neutrons are still produced near the cathode region. In such a state, the neutron production rate still increases in proportion to a power of the discharged current, while if a small sink in the potential is formed at the central region, a double radial peak in the neutron production rate can appear [17].

In figure 10, the radial profiles of (*a*) potential, (*b*) D(d,n)^{3}He fusion reaction rate coefficient and (*c*) reaction rate are shown for presumed ion and electron distribution functions ($\alpha = 0.1$, $\beta_D = 0.05$ and $\xi_D = \xi_e = 1$). The grid voltage is taken as $\phi_0 = 10\,\mathrm{kV}$ and the cathode current is $I_{meas} = 40\,\mathrm{mA}$. We choose somewhat smaller β_e compared with β_D, and we can see the small sink in the central potential (figure 10(*a*)). By using the obtained potential structure, the space-dependent deuteron velocity distribution function $F_D(r, v_\parallel, v_\perp)$ is estimated, and from equation (5), the D(d,n)^{3}He fusion reaction rate coefficient between the accelerated deuterons and the neutral background deuterium gas is evaluated. The fusion reaction rate coefficient obtained is shown in figure 10(*b*). Here, the background gas density is taken as $10^{20}\,\mathrm{m}^{-3}$. Both the relaxations of the velocity distribution function towards an isotropic form and deceleration of ion speed due to the rapid increment in the potential cause the decrement in the fusion reaction rate coefficient near the centre of the sphere. It is shown that the reaction rate coefficient gradually decreases with decreasing r and slightly increases at the centre of the sphere. Multiplying the reaction rate coefficient by accelerated deuteron density and background deuterium one, the D(d,n)^{3}He neutron production rate is evaluated and the result is presented in figure 10(*c*). For small β_D values, the central peak of deuteron density becomes large, while the reaction rate coefficient decreases more rapidly with decreasing r owing to the increment of the potential. The reaction rate coefficient decreases with decreasing r, while the deuteron density increases with deceasing r. When the small potential sink is created at the centre of the sphere, the second peak in the neutron production rate appears near the centre of the sphere in addition to the central peak.

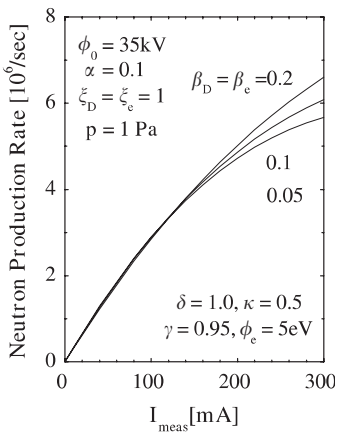

Figure 9. The neutron production rate as a function of discharged current for some $\beta(\equiv \beta_D = \beta_e)$ values.

3.2.3. I^2-scaling of neutron production rate. In this paper, we have introduced a model equation, i.e. equation (1), to express ion and electron distribution functions, and have studied the SIEC device performance, i.e. neutron production rate and its dependence on device parameters. In the previous PIC simulation [18, 19] of SIEC plasmas, however, it has been revealed that the potential oscillates and the frequently oscillated potential behaviour itself plays an important role for device performance. Our treatment (model) is to understand the general characteristics of the SIEC plasmas by looking at instantaneous potential structures for various ion/electron distribution functions. In actual plasmas, charged-particle energy might be transferred between ions and electrons via the oscillated potential, and distribution functions would change their shape. In the PIC simulation [18, 19] the rapid decrement in potential has been observed, which implies existence of the energetic and highly converged electrons. In this section, we perform the calculation by assuming the ion and electron distribution functions whose energy peaks are shifted towards a lower or higher energy range, and explore the mechanism to reproduce the operation mode in which the neutron production rate increases in proportion to more than a power of the discharged current.

At first, to reproduce the double potential well structure, we choose the high electron convergence and take the adjusting parameters as $\alpha = 0.1$, $\beta_D = 0.05$ and $\beta_e = 0.005$. Furthermore, in order to simulate the appearance of energetic electrons, $\xi_e = 1.5$ is assumed. In this calculation, we choose $\xi_D = 0.5$ to avoid the rapid increase in the potential especially near the cathode region. (The effect of the ξ_D parameter is discussed later.) The radial profiles of (*a*) potential, (*b*) D(d,n)^{3}He fusion reaction rate coefficient and (*c*) D(d,n)^{3}He reaction rate are shown in figure 11 for several discharged currents. In the condition where the electron convergence is considerably higher than that of ions and a deep double potential well is formed, the central potential rapidly

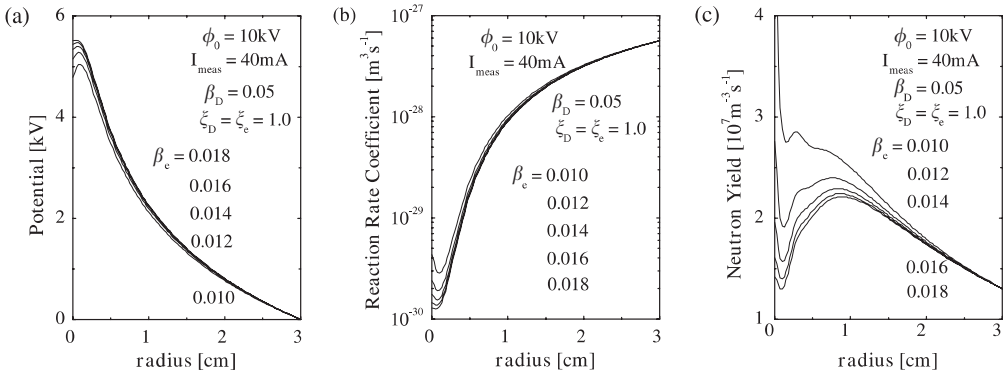

Figure 10. Radial profiles of (*a*) potential, (*b*) D(d,n)^{3}He fusion reaction rate coefficient and (*c*) D(d,n)^{3}He reaction rate, i.e. neutron production rate for several discharged currents.

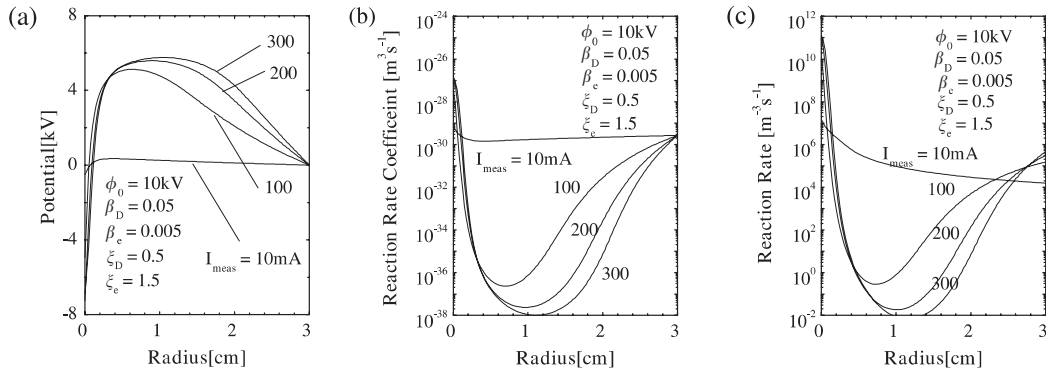

Figure 11. Radial profiles of (*a*) potential, (*b*) D(d,n)^{3}He fusion reaction rate coefficient and (*c*) D(d,n)^{3}He reaction rate for several discharged currents. Here, $\alpha = 0.1$, $\beta_D = 0.05$, $\beta_e = 0.005$, $\xi_D = 0.5$ and $\xi_e = 1.5$ are assumed.

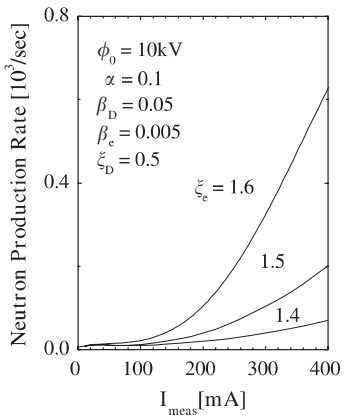

Figure 12. Neutron production rate as a function of discharged current for several ξ_e values.

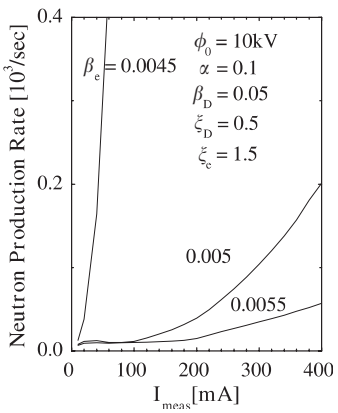

Figure 13. Neutron production rate as a function of discharged current for several electron convergences, i.e. β_e values.

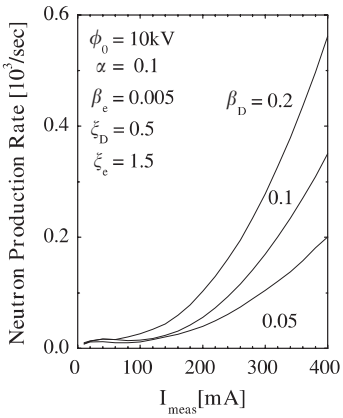

Figure 14. Neutron production rate as a function of discharged current for several deuteron convergences, i.e. β_D values.

decreases with increasing discharged current (see figure 11(*a*)). Here, it should be noted that owing to the decrement in the central potential, ions are accelerated in the velocity space. As a result of the acceleration of ions, the fusion reactivity between ions and background gas rapidly increases around the central core region (see figure 11(*b*)). In such a state, most of the neutrons begin to be produced around the central core region (see figure 11(*c*)), thus contribution of the neutrons produced near the cathode region to total neutron production rate becomes small.

In figure 12, the total neutron production rate from the area within the cathode is plotted as a function of the discharged current for several ξ_e values. For large ξ_e values, energetic electrons appear and create a deeper potential well, and then ions can be more strongly accelerated. As was discussed in the previous section, the depth of the sink in the central potential increases with increasing discharged current as electrons have higher concentration than ions, and relative speed between fuel ions and background gas increases owing to the central sink of the potential. Because the D(d,n)^{3}He fusion cross-section rapidly increases in proportion to more than a power of the relative speed of ions, the total neutron production rate also increases proportional to more than a power of the discharged current, even if most of the neutrons are produced by beam–target fusion reactions. In figure 13 (figure 14) we next show the total neutron production rate as a function of the discharged current for various $\beta_e(\beta_D)$ values. For large $\beta_e(\beta_D)$ values, the electron (ion) concentration in the central core region is weak, and then the degree of the potential sink around the centre of the sphere becomes shallower (more significant). We can find that the neutron production rate decreases (increases) for large $\beta_e(\beta_D)$ values. In frequent potential variation, if the potential is sufficiently lower over the complete radial range and if a deep potential well (virtual cathode) is formed at the central core region, the neutron production rate can increase proportional to more than a power of the discharged current, even if the neutron

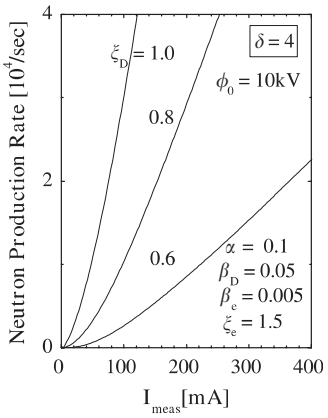

Figure 15. Neutron production rate as a function of discharged current for several ξ_D values. In this case $\delta = 4$ is assumed.

production is sustained mainly by the fusion reactions between the beam (deuteron) and the background (deuterium) gas.

So far, in figures 10–14, in compensation of the appearance of energetic electrons, we have simulated dissipation of the ion energy by using the ξ_D parameter, i.e. $\xi_D = 0.5$. As was discussed in figure 9, when the central peak of the potential is close to externally applied values, the neutron production rate does not increase in proportion to a power of the discharged current. As discussed previously, i.e. figures 10–14, by choosing small ξ_D values, the rapid potential increment has been avoided, and hence the neutron production rate has been smoothly increased with increasing discharged current. It should be noted, however, that as a result of the deceleration of the averaged ion speed, the neutron production rate becomes small. Here, the increased number of the electrons in the area within the cathode can also be considered as another possible mechanism to prevent rapid increase in the potential. We persuade the calculation simulating the higher concentration of the electrons, for example, by choosing the large δ values, i.e. $\delta = 4$. The neutron production rates for several ξ_D values are shown in figure 15 as a function of the discharged current. Here, $\alpha = 0.1$, $\beta_D = 0.05$, $\beta_e = 0.005$ and $\xi_e = 1.5$ are assumed. It is found that owing to the increased deuteron energy, the absolute value of the neutron production rate becomes large for large ξ_D values as obtained in the previous experiment [12], and the neutron production rate remains increasing in proportion to the 1.3–1.6th powers of the discharged current.

4. Concluding remarks

We have studied the correlation between the ion (electron) distribution function and the neutron production in SIEC plasmas by introducing a model equation, i.e. equation (1), to express the ion and electron distribution functions. When ions and electrons have almost the same convergence, or when ions have higher convergence than electrons, the virtual cathode cannot be seen (only the virtual anode is formed). In this case, neutron production in the central core region tends to be relatively small. This is because increased potential, especially in the central core region, prevents the acceleration of ions and the fusion reaction rate coefficient becomes small around the central core region. In such a state, the total neutron production rate does not sensitively depend on the fine structure of the radial profile of the neutron production rate. Since the cathode deuteron density is proportional to the discharged current (see equation (2)), the total neutron production rate linearly increases in proportion to a power of the discharged current. By assuming that the ions and electrons have almost the same convergence, the total neutron production rate and its dependence both on the discharged current and the external voltage are evaluated; and the results are compared with typical experimental data [10, 11]. Although the present model includes several adjustment parameters, transparency factor, the number of secondary electrons emitted from the grid due to ion impact, etc, the calculations almost explain the experiment qualitatively.

If the electron could have higher convergence and energetic component compared with the ion, the virtual cathode would appear, and most of the neutrons would be produced in the central core region. In this state, the discharged current sensitively affects the depth of the central sink of the potential, and the central sink of the potential itself governs the total neutron production. Owing to the rapid increment in relative speed between ions and background gas, fusion reactivity increases. Because the fusion cross-sections increase in proportion to more than a power of the relative speed, the total neutron production also increases in proportion to more than a power of the discharged current, even if most of the neutrons are produced by beam–target fusion reactions. In calculations the I^{1-2}-scaling can more easily appear for small discharged voltage and for large discharged current, i.e. large perveance values, as was reported in previous experiment [12]. This is because the increased current creates a deep central potential well; and the fusion cross-section increases more rapidly for a small energy range. In order to reproduce the scaling of the neutron production rate, (a) energetic electrons and (b) high electron convergence are required in addition to (c) suppressed potential-increment over the complete radial range. In this model, we cannot ascertain whether such a state, i.e. high electron convergence and energy compared with the ions, can appear or not; however, previous experiment [12, 15] and PIC simulation [18] suggest the appearance of the condition. In order to further improve the device performance, it would be necessary to ascertain whether such a condition, i.e. double potential well formation, can really exist and to examine how we can reproduce such a state.

In this paper, the characteristics of the SIEC device are examined by looking at the instantaneous plasma state for various combinations of non-equilibrium ion/electron distribution functions. The neutrons from the laboratory devices would be produced in dynamically equilibrium plasmas where the potential structure is formed and collapsed at a high frequency [18]. In laboratory devices, angular momentum is imparted by non-uniform surfaces around the grid and/or the ion source, thus time-averaged momentum distribution of ions may be broadened. In previous simulation [25], it was reported that a non-zero angular momentum might be desirable in some cases to control/expand the volume of the potential well. This result agreed well with our model. In our model, the I^{1-2}-scaling can more easily appear for large β_D. This is because owing to the increase in perpendicular

ion energy component, the central potential decreases and the depth of the central potential well becomes large.

In most of the present calculations the number of secondary electrons emitted from the grid due to ion impact is assumed to be unity, i.e. $\delta = 1$. If the number of electrons within the cathode increases, the potential would not be increased so much. In such a state, since the deceleration of the fuel-ion speed becomes small, the I^{1-2}-scaling of the neutron production would appear for lower ion convergences than those in figures 12–15. Furthermore, if ion convergences were lower than those in figures 12–15, a similar I^{1-2}-scaling would be obtained for lower electron convergences. In our treatment (present model), we have only studied the static plasma characteristics for various ion/electron convergences. In parallel with this type of calculation, the simulation to investigate the distribution function itself would also be necessary. In our model, the effect of the charge-exchange process has not been included (although energy dissipation of the ion distribution function due to the charge-exchange processes [24] can be simulated by using the α and ξ parameters). The importance of the charge-exchange collisions have been pointed out by Thorson *et al* [22], and they have shown that the collisions can enhance the fusion reaction rate. In order to know the fuel-ion distribution function in laboratory SIEC devices and how the distribution is influenced by the device parameters, the bounce-averaged Boltzmann–Fokker–Planck analysis would be an effective numerical approach. By coupling the present treatment with the kinetic simulation considering the interaction between ions and electrons via variation of the electrostatic potential, more detailed dynamics of SIEC plasmas can be clarified.

Acknowledgments

This work was motivated when the first author was at the University of Illinois. We gratefully acknowledge Prof. G.H. Miley for offering plenty of information about SIEC. Special thanks go to Prof. M. Ohnishi and Prof. K. Yoshikawa for continued discussions and advices. The authors also acknowledge Dr R.L. Hirsch and Prof. H. Momota for useful comments and helpful discussions at the '5th US-Japan Workshop on IEC Proton/Neutron Sources', October 2002, Madison, USA.

We wish to acknowledge partial support for this work from the Kyushu Electric Power Co. and the Computational Cooperative program of the National Institute for Fusion Science.

References

[1] Thorson T.A., Durst R.D., Fonck R.J. and Wainwrite L.P. 1997 *Phys. Plasmas* **4** 4
[2] Hirsh R.L. 1968 *Phys. Fluids* **11** 2486
[3] Kulcinski G.L. 1998 *Fusion Technol.* **34** 477
[4] Ashley R.P. *et al* 2002 Recent IEC experimental results at the University of Wisconsin *4th US-Japan Workshop on IEC Neutron Sources (Kyoto, Japan, March 2002)* submitted
[5] Ashley R.P. *et al* 2001 *Fusion Technol.* **39** 546
[6] Momota H., Miley G.H. and Nadler J. 2000 *Direct Energy Convergion for IEC Propulsions* (Toki, Japan: National Institute for Fusion Science) NIFS-641
[7] Miley G.H., Momota H., Shaban Y. and Hora H. 2002 Progress in development of a converging beam neutron source for driving a sub-critical fission reactor *10th Int. Conf. on Nuclear Engineering (Arlington, VA, April 2002)* paper #22149 (ASME publication)
Miley G.H. *et al* 2002 *German Patent* 432792 C2
[8] Dautray R. 1993 Commentaires sur la proposition de Carlo RUBBIA d'amplificateur d'energy *Report* LE HAUT-COMISSAIRE CHC/93-104 (3 December 1993)
[9] Hirsh R.L. 1967 *J. Appl. Phys.* **38** 4522
[10] Miley G.H., Gu Y., DeMora J. and Ohnishi M. 1998 *Fusion Eng. Des.* **41** 461
[11] Miley G.H. *et al* 1991 *Fusion Technol.* **19** 840
[12] Gu Y., Williams M., Stubbers R. and Miley G.H. 1996 *Fusion Technol.* **30** 1342
[13] Gu Y. and Miley G.H. 2000 Experimental study of potential structure in a spherical IEC device *IEEE Trans. Plasma Sci.* **28** 331
[14] Hora H. 2002 *Innovation, Technologie und Okonomie (Regensburg)* 2nd edn, ed S. Roderer, p 37
[15] Yoshikawa K. *et al* 2001 *Nucl. Fusion* **41** 717
[16] Matsuura H., Takaki T., Nakao Y. and Kudo K. 2001 *Fusion Technol.* **39** 1167
[17] Matsuura H., Takaki T., Funakoshi K., Nakao Y. and Kudo K. 2000 *Nucl. Fusion* **40** 1951
[18] Ohnishi M., Sato K.H., Yamamoto Y. and Yoshikawa K. 1997 *Nucl. Fusion* **37** 611
[19] Ohnishi M. *et al* 1998 *Fusion Technol.* **34** 1071
[20] Nevins W. 1995 *Phys. Plasmas* **2** 3804
[21] Momota H. and Miley G.H. 2001 *Fusion Sci. Technol.* **40** 56
[22] Thorson T.A., Durst R.D., Fonck R.J. and Sontag A.C. 1998 *Nucl. Fusion* **38** 495
[23] Duane B.H. 1972 *Fusion Cross-Section Theory* BNWL-1685, Battelle Pacific Northwest Laboratories
[24] Santarius J.F. *et al* 2002 Modeling D-D Operation of the UW IEC Experiment *5th US-Japan Workshop on IEC Fusion (Madison, USA, October 2002)* submitted
[25] Tzonev I.V. *et al* 1996 Effect of large ion angular momentum spread and high current on inertial electrostatic confinement potential structures *16th IEEE/NPSS Symp. on Fusion Engineering, IEEE No 95 CH35852, IEEE (Piscataway, NJ, 1996)* ed G.H. Miley and C.M. Elliott, p 1476